

QCD equation of state via the complex Langevin method

Felipe Attanasio

Institute for Theoretical Physics, Universität Heidelberg, Philosophenweg 16, D-69120, Germany

Benjamin Jäger

*CP3-Origins & Danish IAS, Department of Mathematics and Computer Science,
University of Southern Denmark, Campusvej 55, 5230 Odense M, Denmark*

Felix P.G. Ziegler

*CP3-Origins & Danish IAS, Department of Mathematics and Computer Science,
University of Southern Denmark, Campusvej 55, 5230 Odense M, Denmark and
School of Physics and Astronomy, The University of Edinburgh, EH9 3FD Edinburgh, United Kingdom*

We present lattice simulations on the phase diagram of Quantum Chromodynamics (QCD) with two light quark flavours at finite chemical potential μ . To circumvent the sign problem we use the complex Langevin method. In this study, we have carried out ab-initio lattice QCD calculations at finite density for a pion mass of ~ 480 MeV. We report on the pressure, energy and entropy equations of state, as well as the observation of the Silver Blaze phenomenon.

I. INTRODUCTION

Revealing the phase diagram of *Quantum Chromodynamics* (QCD) from first principles is one of the big challenges in modern high energy physics. Insight into the hot and dense strongly interacting quark-gluon plasma (QGP) phase provides answers to the physics of the early universe and supernovae. Complementary, the cold and dense regions exhibiting a rich structure of hadronic matter contain crucial information for the understanding of neutron stars. Exploring QCD at finite temperature and baryon density is of paramount importance in heavy-ion collision experiments at LHC, RHIC, FAIR, and NICA. On the theory side the lattice formulation of QCD offers a well-established numerical framework to compute the QCD phase diagram from first principles.

The phase structure, including nature and critical temperature of the chiral and deconfinement transitions, is well understood at vanishing chemical potential [1, 2]. A finite chemical potential, $\mu > 0$, renders the Euclidean action and hence the path-integral measure complex, thus prohibiting the use of conventional Monte Carlo simulations. Moreover, reweighting the phase of the fermion determinant comes with exponential simulation costs as the lattice volume increases. This is the sign problem in lattice QCD. Over the last two decades various solution programs to deal with the sign problem have been established [3]. Among its candidates rank a variety of reweighting methods [4, 5], Taylor expansions [6, 7] and analytic continuation from imaginary chemical potential [8–11], dual formulations and the density of states method [12]. Complementary, the complex Langevin (CL) method [13, 14] as well as the Lefschetz thimble method and generalizations thereof [15] are based on analytic continuation in the field variables into the non-compact gauge group $SL(3, \mathbb{C})$. A recent overview of lattice efforts to compute the QCD phase diagram can be found in [16].

In this work, we present results on the phase diagram and the extraction of the equation of state of QCD with two mass-degenerate light flavors. In particular, we focus on exploring the phase diagram in the region of low temperature and finite density. The latter gives rise to a particularly severe sign problem. Our approach to cope with this is the complex Langevin method. Over the last decade, a plethora of tools to guarantee stability and correctness in CL simulations has been developed, see e.g. [17–25]. Here we put those tools to work in QCD with dynamical quarks and low temperatures.

Our CL-based approach allows us to investigate a large portion of the phase diagram, in particular with baryon chemical potentials close to and above the nucleon mass. The focus of this work is on temperatures between 50 MeV and 200 MeV and baryon chemical potential up to twice the nucleon mass, complementing previous studies of the QCD phase diagram [26–32] and equation of state [5, 7, 33–39]. Our simulations have been performed at fixed volume and lattice spacing, with pions lighter than 500 MeV. We present here the pressure, energy and entropy equations of state (EoS) in the $T - \mu$ plane, and also numerical evidence of the Silver Blaze phenomenon [40]. Other studies of the QCD phase diagram via complex Langevin simulations can be found in [41–45].

II. COMPUTATIONAL METHOD

Our simulations have been performed in the grand-canonical ensemble by employing the complex Langevin method. This technique allows the circumvention of the sign problem by extending the configuration space for the gauge link variables from the group $SU(3)$ to $SL(3, \mathbb{C})$. Complex Langevin has been successfully used in tackling the sign problem, beyond the above cited cases, in the relativistic Bose gas [46], polarized [47] and mass-imbalanced [48] ultracold atoms. For recent reviews, see [14, 49].

We use the standard Wilson plaquette gauge action

$$S_g = \frac{\beta}{3} \sum_x \sum_{\mu < \nu} \text{Tr} \left[\mathbb{1} - \frac{1}{2} (U_{x,\mu\nu} + U_{x,\mu\nu}^{-1}) \right], \quad (1)$$

where $U_{x,\mu\nu}$ represents the elementary plaquette at site x in the directions μ and ν , and β is the inverse coupling. The quark contribution is given by the action for N_f flavors of unimproved Wilson fermions

$$S_f = -N_f \text{Tr} \log M(U, \mu), \quad (2)$$

with the Dirac operator

$$M_{xy} = (4 + m)\delta_{xy} - \frac{1}{2} \sum_{\nu} \left[\Gamma_{\nu} e^{\mu\delta_{\nu,0}} U_{x,\nu} \delta_{x+\hat{\nu},y} + \Gamma_{-\nu} e^{-\mu\delta_{\nu,0}} U_{x-\hat{\nu},\nu}^{-1} \delta_{x-\hat{\nu},y} \right]. \quad (3)$$

The parameters m and μ stand for the quark mass and chemical potential, respectively, in lattice units, and $\Gamma_{\pm\nu} = 1 \mp \gamma_{\nu}$.

Field configurations are generated using the complex Langevin [50, 51] method

$$U_{x,\mu}(\theta + \epsilon) = \exp \left[\epsilon \lambda^a \left(-D_{x,\mu}^a S + \eta_{x,\mu}^a \right) \right] U_{x,\mu}(\theta), \quad (4)$$

where $\eta_{x,\mu}^a$ are white noise fields and the derivative in the Langevin drift, $K_{x,\mu}^a \equiv -D_{x,\mu}^a S$, acts on the group manifold [13, 52]. The step size ϵ is changed adaptively during the simulation [53], and we make use of the gauge cooling technique [17] to reduce large explorations of the (non-compact) group manifold. Our drift is augmented with the dynamical stabilisation term to help ensuring proximity to the $SU(3)$ manifold [22]. Quantum expectation values are averages for large θ . We have estimated autocorrelation times following [54].

Our CL simulation code is based on the openQCD [55] and openQCD-fastsum software packages [56]. The most costly part of the CL simulation is the computation of the fermionic drift force. The quark contribution to the Langevin drift reads

$$(K_{x,\mu}^a)_{\text{quark}} = N_f \text{Tr} \left[M^{-1} D_{x,\mu}^a M \right]. \quad (5)$$

We have used the even-odd preconditioned conjugate gradient routine in [55] applied to the normal equation $M^\dagger M \psi = \eta$ to estimate M^{-1} , and compute the trace using the bilinear noise scheme. To reduce the numerical effort further, we update the gauge force more frequently than the fermionic drift. We choose the ratio of gauge over fermion updates to be 16. This needs to be taken into consideration once we conduct the step size extrapolation. As a reference, we carried out a finite-step extrapolation for vanishing chemical potential in [57]. Here results are shown for an average step size of the order of $\mathcal{O}(10^{-3})$.

III. NUMERICAL RESULTS

We present results in dimensionless ratios. We have also measured the Polyakov loop,

$$P = \frac{1}{3V} \sum_{\vec{x}} \text{Tr} \left\langle \prod_{\tau} U_{(\vec{x},\tau),\hat{0}} \right\rangle, \quad (6)$$

where the product is taken along the periodic Euclidean time direction, and quark number density

$$\langle n \rangle = \frac{1}{N_{\tau} V} \frac{\partial \ln Z}{\partial \mu}. \quad (7)$$

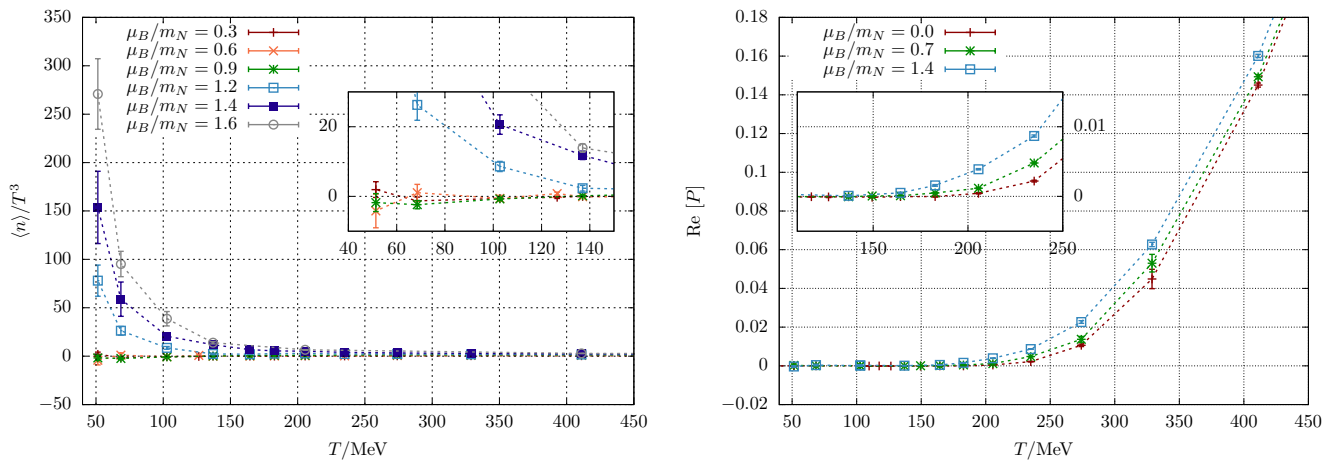


FIG. 1. Quark number density (left) and real part of the Polyakov loop (right) as functions of temperature for different baryonic chemical potentials. Remnants of the Silver Blaze effect can be seen in the density plot. The inset on the density plot zooms into the lower temperature, low density region and shows that for $\mu_B > m_N$ the density decreases slower than T^3 for small temperatures. In the Polyakov loop plot, the inset focuses on the region where $\text{Re}[P]$ starts differing from zero. The Polyakov loop, despite not being an order parameter in QCD, still serves as an indicator of confinement. Dashed lines are to guide the eye. Error bars are statistical only.

Other thermodynamic quantities, such as pressure, energy, and entropy are discussed in the next section.

Our simulations have been performed at a fixed lattice spacing of $a \sim 0.06$ fm [58], a spatial volume of $V = 24^3$ in lattice units, and a quark bare hopping parameter of $\kappa = 0.1544$, and inverse coupling $\beta = 5.8$. These input values correspond to pion and nucleon masses of $m_\pi \approx 480$ MeV and $m_N \approx 1.3$ GeV. The value of the stabilisation parameter α_{DS} has been chosen such that its impact on the observables is minimal [22].

We have scanned the $T - \mu$ plane by varying the quark chemical potential in the range $0 \leq a\mu \leq 0.28$ in steps of 0.02 and $4 \leq N_t \leq 64$, corresponding to $0.0 \lesssim \mu \lesssim 920$ MeV and $50 \text{ MeV} \lesssim T \lesssim 820$ MeV, respectively. With this type of scan our simulations cover both hadronic and quark-gluon plasma regions, as well as regions of pion and nucleon condensation. Since we work with two degenerate flavors, a finite pion density cannot be observed by increasing the quark chemical potential. However, it is expected that for temperatures below the deconfinement transition a non-vanishing quark density should appear for $\mu \gtrsim m_N/3$. In particular, at $T = 0$ the quark density should vanish for $\mu < m_N/3$. This is known as the *Silver Blaze* phenomenon [40], a peculiar situation where the *absence* of net quark density for $0 \leq \mu < m_N/3$ is actually due to non-trivial cancellation between eigenmodes of the Dirac operator. Information about the deconfinement transition can be obtained from the Polyakov loop, even though it is only an order parameter in purely gluonic theories. A vanishing Polyakov loop indicates the absence of free quarks, while a non-zero value implies the reverse.

We present in fig. 1 the quark number density and Polyakov loop as functions of the temperature. The density plot clearly shows direct evidence of the Silver Blaze phenomenon: for $\mu_B > m_N$ the data shows $\langle n \rangle / T^3$ diverging, indicating that $\langle n \rangle$ remains finite as the temperature decreases. Conversely, for $\mu_B < m_N$ the density decreases faster than T^3 for low temperatures. Strictly speaking, the Silver Blaze phenomenon only happens at zero temperature, but the plot shows that for simulations performed below the baryon condensation threshold, $\mu_B < m_N$, the density tends to zero as the temperature decreases, while for $\mu_B > m_N$ it remains finite. The confinement of quarks is indicated by the average Polyakov loop: the figure shows that quarks become free at lower temperatures for larger chemical potentials. This is in accordance with the traditional expected picture of the QCD phase diagram.

IV. EQUATION OF STATE

The pressure equation of state can be obtained via

$$\Delta p(\mu_B, T) = \int_0^{\mu_B} d\mu' \langle n(\mu', T) \rangle \quad (8)$$

In order to perform the integration, the density as a function of the chemical potential was fitted by a cubic polynomial for each temperature, shown in fig. 2 (left). The uncertainty on the fit coefficients has been used to compute 1σ error

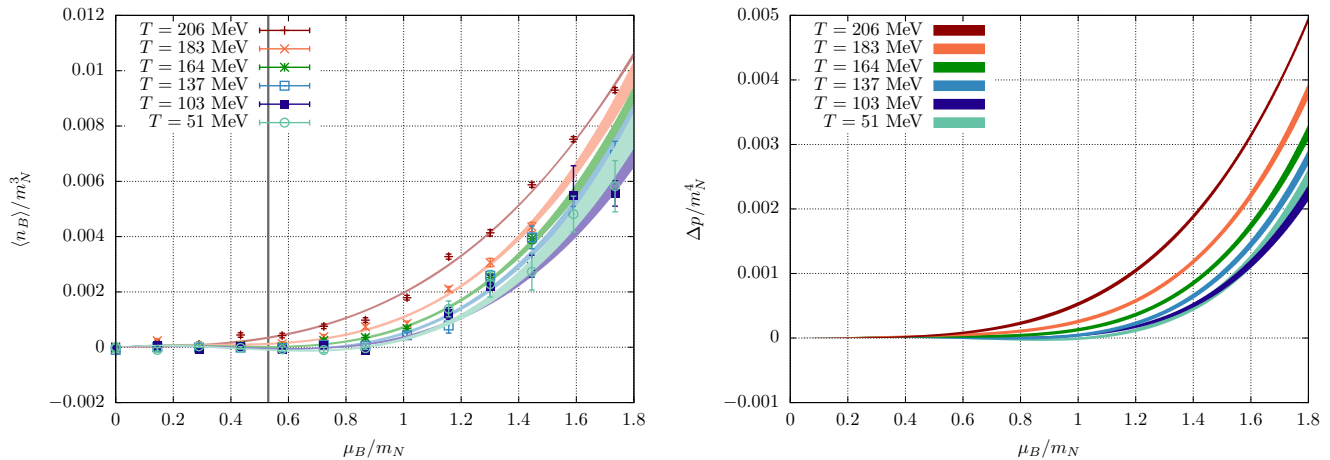


FIG. 2. Baryon density normalized by the nucleon mass, and pressure in units of temperature, as functions of the baryon chemical potential. The density plot includes polynomial fits for each temperature. The vertical line indicates $\mu = m_\pi/2$ for reference.

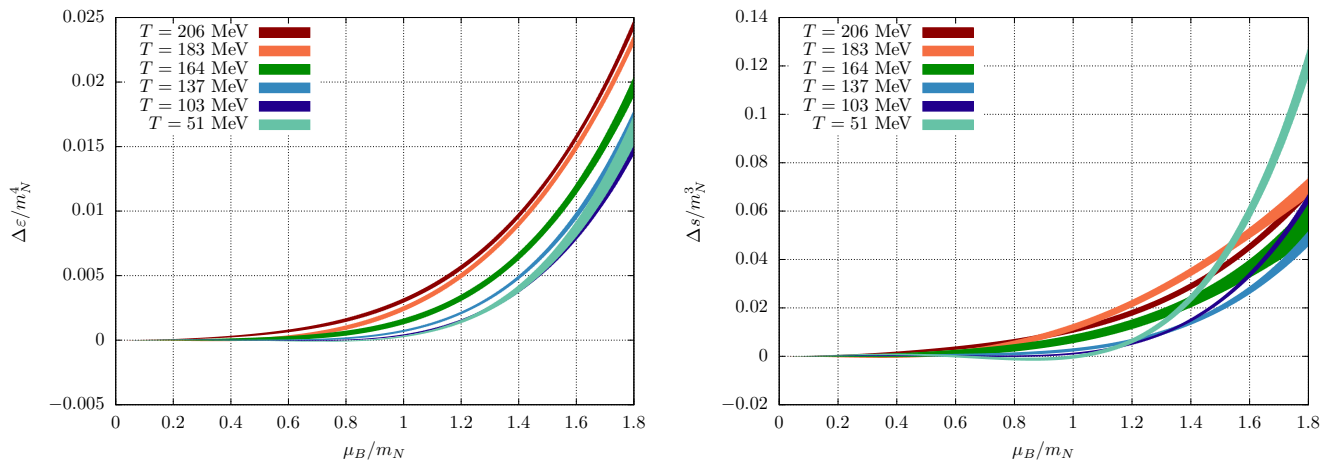


FIG. 3. Energy and entropy densities, in units of the nucleon mass, as functions of the baryon chemical potential.

bands. The choice of cubic polynomial was inspired by a phenomenological parametrization of the pressure equation of state for quark matter, see e.g. [59], in terms of a quartic polynomial in μ . Similar studies have been carried out using isospin, rather than baryon, chemical potential, where the viability of compact pion stars [60], and QCD thermodynamics [38] have been investigated.

Using the pressure equation of state we have computed the trace anomaly,

$$\frac{\Delta I}{T^4} = T \frac{\partial}{\partial T} \left[\frac{p(\mu_B, T)}{T^4} \right] + \frac{\mu_B n_B(\mu_B, T)}{T^4}, \quad (9)$$

where $n_B = n/3$ is the baryon number density, and subsequently the energy and entropy densities,

$$\Delta \epsilon = \Delta I + 3\Delta p, \quad (10)$$

$$T\Delta s = \Delta \epsilon + \Delta p - \mu n, \quad (11)$$

respectively. The derivative inside the trace anomaly has been computed numerically, using the fit coefficients of the pressure computed at each fixed temperature.

The pressure difference with respect to the $\mu_B = 0$ case is displayed in fig. 2 (right), whence a growth can be observed as a function of μ_B . For our lowest temperature it is noticeable that this growth really only starts at $\mu_B = m_N$, since prior to that the baryon number density is essentially zero. The energy and entropy densities can be found in fig. 3. An increase in the energy density difference as μ_B grows is clearly visible for all temperatures

considered. In particular, as expected from the nearly vanishing quark number density at low temperatures and chemical potential, $\Delta\varepsilon$ only starts to deviate from zero for $\mu_B \gtrsim m_N$. For the higher temperatures the growth starts much sooner.

The stiffness of the equation of state can be inferred from the density as a function of μ_B , shown in the right panel of fig. 2. It grows slower for lower temperatures, implying that the EoS becomes stiffer as T decreases.

V. SUMMARY AND OUTLOOK

We have presented ab-initio results of the QCD phase diagram with relatively light pions ($\lesssim 480$ MeV) in the $T - \mu$ plane. We cover a baryon number density range of up to ~ 15 times the nuclear saturation density $n_0 \simeq 0.16 \text{ fm}^{-3}$ at $T \sim 50$ MeV and up to $\sim 20n_0$ at $T \sim 200$ MeV. At low temperatures we observe remnants of the Silver Blaze phenomenon, where the quark number density vanishes at $T = 0$ for $\mu < m_N/3$. Our results also show that the pressure equation of state becomes stiffer for lower temperatures. This is in accordance with the behavior necessary for the stability of neutron stars [61].

In order to further understand dense nuclear matter, our future plans include the addition of the strange quark to our simulations. This would be of particular relevance to studies of neutron stars, as they are known to soften the equation of state. Additionally, our results have been obtained at a finite lattice spacing and need to be continuum and finite step size extrapolated. We plan on employing improved actions to improve the approach to the continuum limit. Another interesting point is the search for the critical end-point (CEP), which requires a fine scan of the phase diagram as well as finite volume scaling analyses and finite step size extrapolation.

VI. ACKNOWLEDGMENTS

We are grateful for discussions with Gert Aarts and Ion-Olimpiu Stamatescu. Part of the computing resources for this work were provided by U. of Southern Denmark and DeiC Interactive HPC (Ucloud, GenomeDK). Furthermore, this work was performed using PRACE resources at Hawk (Stuttgart) with project ID 2018194714. This work used the DiRAC Extreme Scaling service at the University of Edinburgh, operated by the Edinburgh Parallel Computing Centre on behalf of the STFC DiRAC HPC Facility (www.dirac.ac.uk). The work of F.A. was supported by the Deutsche Forschungsgemeinschaft (DFG, German Research Foundation) under Germany's Excellence Strategy EXC2181/1 - 390900948 (the Heidelberg STRUCTURES Excellence Cluster) and under the Collaborative Research Centre SFB 1225 (ISOQUANT).

-
- [1] H. T. Ding *et al.* (HotQCD), Phys. Rev. Lett. **123**, 062002 (2019), arXiv:1903.04801 [hep-lat].
 - [2] S. Borsanyi, Z. Fodor, C. Hoelbling, S. D. Katz, S. Krieg, C. Ratti, and K. K. Szabo (Wuppertal-Budapest), JHEP **09**, 073, arXiv:1005.3508 [hep-lat].
 - [3] P. de Forcrand, *Proceedings, 27th International Symposium on Lattice field theory (Lattice 2009): Beijing, P.R. China, July 26-31, 2009*, PoS **LAT2009**, 010 (2009), arXiv:1005.0539 [hep-lat].
 - [4] Z. Fodor and S. D. Katz, JHEP **03**, 014, arXiv:hep-lat/0106002.
 - [5] S. Borsanyi, Z. Fodor, M. Giordano, S. D. Katz, D. Nogradi, A. Pasztor, and C. H. Wong (2021) arXiv:2108.09213 [hep-lat].
 - [6] C. R. Allton, S. Ejiri, S. J. Hands, O. Kaczmarek, F. Karsch, E. Laermann, C. Schmidt, and L. Scorzato, Phys. Rev. **D66**, 074507 (2002), arXiv:hep-lat/0204010 [hep-lat].
 - [7] S. Borsányi, Z. Fodor, J. N. Guenther, R. Kara, S. D. Katz, P. Parotto, A. Pásztor, C. Ratti, and K. K. Szabó, Phys. Rev. Lett. **126**, 232001 (2021), arXiv:2102.06660 [hep-lat].
 - [8] P. de Forcrand and O. Philipsen, Nucl. Phys. **B642**, 290 (2002), arXiv:hep-lat/0205016 [hep-lat].
 - [9] M. D'Elia and M.-P. Lombardo, Phys. Rev. D **67**, 014505 (2003), arXiv:hep-lat/0209146.
 - [10] A. Collaboration, Physics Letters B **716**, 1 (2012).
 - [11] P. Dimopoulos, L. Dini, F. Di Renzo, J. Goswami, G. Nicotra, C. Schmidt, S. Singh, K. Zambello, and F. Ziesché, Phys. Rev. D **105**, 034513 (2022), arXiv:2110.15933 [hep-lat].
 - [12] C. Gatttringer and K. Langfeld, Int. J. Mod. Phys. **A31**, 1643007 (2016), arXiv:1603.09517 [hep-lat].
 - [13] G. Aarts and I.-O. Stamatescu, JHEP **09**, 018, arXiv:0807.1597 [hep-lat].
 - [14] F. Attanasio, B. Jäger, and F. P. G. Ziegler, Eur. Phys. J. A **56**, 251 (2020), arXiv:2006.00476 [hep-lat].
 - [15] A. Alexandru, G. Basar, P. F. Bedaque, and N. C. Warrington, (2020), arXiv:2007.05436 [hep-lat].
 - [16] J. N. Guenther, Eur. Phys. J. A **57**, 136 (2021), arXiv:2010.15503 [hep-lat].
 - [17] E. Seiler, D. Sexty, and I.-O. Stamatescu, Phys. Lett. **B723**, 213 (2013), arXiv:1211.3709 [hep-lat].
 - [18] K. Nagata, J. Nishimura, and S. Shimasaki, PTEP **2016**, 013B01 (2016), arXiv:1508.02377 [hep-lat].

- [19] J. Nishimura and S. Shimasaki, Phys. Rev. **D92**, 011501 (2015), arXiv:1504.08359 [hep-lat].
- [20] K. Nagata, J. Nishimura, and S. Shimasaki, Phys. Rev. **D94**, 114515 (2016), arXiv:1606.07627 [hep-lat].
- [21] G. Aarts, E. Seiler, D. Sexty, and I.-O. Stamatescu, JHEP **05**, 044, arXiv:1701.02322 [hep-lat].
- [22] F. Attanasio and B. Jäger, Eur. Phys. J. **C79**, 16 (2019), arXiv:1808.04400 [hep-lat].
- [23] K. Nagata, J. Nishimura, and S. Shimasaki, JHEP **05**, 004, arXiv:1802.01876 [hep-lat].
- [24] M. Scherzer, E. Seiler, D. Sexty, and I. O. Stamatescu, Phys. Rev. **D101**, 014501 (2020), arXiv:1910.09427 [hep-lat].
- [25] E. Seiler, Phys. Rev. D **102**, 094507 (2020), arXiv:2006.04714 [hep-lat].
- [26] V. Vovchenko, J. Steinheimer, O. Philipsen, and H. Stoecker, Phys. Rev. D **97**, 114030 (2018), arXiv:1711.01261 [hep-ph].
- [27] B. B. Brandt, G. Endrodi, and S. Schmalzbauer, Phys. Rev. D **97**, 054514 (2018), arXiv:1712.08190 [hep-lat].
- [28] A. Bazavov *et al.* (HotQCD), Phys. Lett. B **795**, 15 (2019), arXiv:1812.08235 [hep-lat].
- [29] B. B. Brandt, F. Cuteri, G. Endrodi, and S. Schmalzbauer, PoS **LATTICE2019**, 189 (2019), arXiv:1911.12197 [hep-lat].
- [30] O. Philipsen and J. Scheunert, PoS **LATTICE2019**, 206 (2019), arXiv:1912.01724 [hep-lat].
- [31] S. Borsanyi, Z. Fodor, J. N. Guenther, R. Kara, S. D. Katz, P. Parotto, A. Pasztor, C. Ratti, and K. K. Szabo, Phys. Rev. Lett. **125**, 052001 (2020), arXiv:2002.02821 [hep-lat].
- [32] O. Philipsen, Indian J. Phys. **95**, 1599 (2021), arXiv:2104.03696 [hep-lat].
- [33] S. Borsányi, Z. Fodor, C. Hoelbling, S. D. Katz, S. Krieg, and K. K. Szabo, Phys. Lett. **B730**, 99 (2014), arXiv:1309.5258 [hep-lat].
- [34] A. Bazavov *et al.* (HotQCD), Phys. Rev. D **90**, 094503 (2014), arXiv:1407.6387 [hep-lat].
- [35] A. Bazavov *et al.*, Phys. Rev. D **95**, 054504 (2017), arXiv:1701.04325 [hep-lat].
- [36] V. Vovchenko, J. Steinheimer, O. Philipsen, and H. Stoecker, PoS **CORFU2018**, 199 (2019), arXiv:1905.01031 [hep-ph].
- [37] V. Vovchenko, B. B. Brandt, F. Cuteri, G. Endródi, F. Hajkarim, and J. Schaffner-Bielich, Phys. Rev. Lett. **126**, 012701 (2021), arXiv:2009.02309 [hep-ph].
- [38] B. B. Brandt, F. Cuteri, and G. Endrodi, in *38th International Symposium on Lattice Field Theory* (2021) arXiv:2110.14750 [hep-lat].
- [39] P. Parotto, S. Borsanyi, Z. Fodor, J. N. Guenther, R. Kara, S. D. Katz, A. Pasztor, C. Ratti, and K. K. Szabo, in *38th International Symposium on Lattice Field Theory* (2021) arXiv:2112.00083 [hep-lat].
- [40] T. D. Cohen, Phys. Rev. Lett. **91**, 222001 (2003), arXiv:hep-ph/0307089 [hep-ph].
- [41] D. Sexty, Phys. Lett. **B729**, 108 (2014), arXiv:1307.7748 [hep-lat].
- [42] G. Aarts, F. Attanasio, B. Jäger, and D. Sexty, JHEP **09**, 087, arXiv:1606.05561 [hep-lat].
- [43] D. Sexty, Phys. Rev. **D100**, 074503 (2019), arXiv:1907.08712 [hep-lat].
- [44] M. Scherzer, D. Sexty, and I. O. Stamatescu, Phys. Rev. D **102**, 014515 (2020), arXiv:2004.05372 [hep-lat].
- [45] S. Tsutsui, Y. Asano, Y. Ito, H. Matsufuru, Y. Namekawa, J. Nishimura, A. Tsuchiya, and T. Yokota, in *38th International Symposium on Lattice Field Theory* (2021) arXiv:2111.15095 [hep-lat].
- [46] G. Aarts, Phys. Rev. Lett. **102**, 131601 (2009), arXiv:0810.2089 [hep-lat].
- [47] A. C. Loheac and J. E. Drut, Phys. Rev. **D95**, 094502 (2017), arXiv:1702.04666 [hep-lat].
- [48] L. Rammelmüller, J. E. Drut, and J. Braun, SciPost Phys. **9**, 014 (2020), arXiv:2003.06853 [cond-mat.quant-gas].
- [49] C. E. Berger, L. Rammelmüller, A. C. Loheac, F. Ehmman, J. Braun, and J. E. Drut, Phys. Rept. **892**, 1 (2021), arXiv:1907.10183 [cond-mat.quant-gas].
- [50] G. Parisi and Y.-s. Wu, Sci. Sin. **24**, 483 (1981).
- [51] G. Parisi, Physics Letters B **131**, 393 (1983).
- [52] P. H. Damgaard and H. Hüffel, Phys. Rept. **152**, 227 (1987).
- [53] G. Aarts, L. Bongiovanni, E. Seiler, D. Sexty, and I.-O. Stamatescu, Eur. Phys. J. **A49**, 89 (2013), arXiv:1303.6425 [hep-lat].
- [54] U. Wolff (ALPHA), Comput. Phys. Commun. **156**, 143 (2004), [Erratum: Comput. Phys. Commun.176,383(2007)], arXiv:hep-lat/0306017 [hep-lat].
- [55] <https://luscher.web.cern.ch/luscher/openQCD/> (2020).
- [56] <https://fastsum.gitlab.io/> (2020).
- [57] F. Attanasio, B. Jäger, and F. P. G. Ziegler, in *38th International Symposium on Lattice Field Theory* (2021) arXiv:2111.02241 [hep-lat].
- [58] L. Del Debbio, L. Giusti, M. Luscher, R. Petronzio, and N. Tantalo, JHEP **02**, 011, arXiv:hep-lat/0512021.
- [59] M. Alford, M. Braby, M. W. Paris, and S. Reddy, Astrophys. J. **629**, 969 (2005), arXiv:nucl-th/0411016.
- [60] B. B. Brandt, G. Endrodi, E. S. Fraga, M. Hippert, J. Schaffner-Bielich, and S. Schmalzbauer, Phys. Rev. D **98**, 094510 (2018), arXiv:1802.06685 [hep-ph].
- [61] G. Baym, T. Hatsuda, T. Kojo, P. D. Powell, Y. Song, and T. Takatsuka, Rept. Prog. Phys. **81**, 056902 (2018), arXiv:1707.04966 [astro-ph.HE].